A Combined Circuit-FEM Model of HTS Power Cables for Their Analysis During Critical Transients

Mattia Simonazzi, *Member, IEEE*, Antonio Morandi, *Senior Member, IEEE*, Fedor Gomory, *Senior Member, IEEE*, Eugen Seiler, Marek Mošať, Emiliano Guerra, Francesco Mimmi, and Massimo Fabbri

***Abstract*—The paper discusses the development and application of circuit models for superconducting DC power cables to investigate their interaction with the power system. These models, created as part of the SCARLET project, simulate the behaviour of different cable components (e.g., HTS layers, shield, cryopipes) during power system transients like energization and faults. By integrating these models with power system simulators, accurate current profiles of the cable components are obtained. Additionally, the paper introduces a combined circuit and 2D finite element method (FEM) model to study the electro-thermal behaviour of the cable. The circuit model is developed to account for all the relevant factors like the E-J power-law characteristic, the magnetic field's influence on the superconductor and heat generation. Then the FEM model provides the detailed electro-thermal behaviour of the cable components considering the current profiles obtained from the circuit model as input, enabling efficient and focused simulation of localized effects without the computational complexity of fully coupled simulations. Using this combined model, the performance of a reference HTS cable under a pole-to-pole fault is analysed. Results show a limited temperature increase during transients, including both energization and fault scenarios, with peaks of only fractions of a Kelvin occurring immediately after the pole-to-pole fault. The FEM model further provides detailed temperature maps, illustrating the corresponding temperature distribution throughout the cable components, proving the save operation on post restoration.**

***Index Terms*—DC microgrid, high temperature superconductors, power systems, superconducting cables, smart grid, transient analysis.**

Received 1 October 2024; revised 14 January 2025; accepted 8 February 2025. Date of publication 3 March 2025; date of current version 20 March 2025. This work was supported in part by the European Union's Horizon Europe Research and Innovation Programme SCARLET under Grant 101075602101075602, in part by the EU Next Generation EU - NEST (Network 4 Energy Sustainable Transition) SPOKE 7 and ECOSISTER SPOKE 4 under Grant PNRR - M4C2 - I1.3, and in part by the Recovery and Resilience Plan for Slovakia under Grant 09I01-03-V04-00020. *(Corresponding author: Mattia Simonazzi.)*

Mattia Simonazzi, Antonio Morandi, Emiliano Guerra, Francesco Mimmi, and Massimo Fabbri are with the Department of Electrical, Electronic and Information Engineering "Guglielmo Marconi" of the University of Bologna, 40126 Bologna, Italy (e-mail: mattia.simonazzi2@unibo.it).

Fedor Gomory, Eugen Seiler, and Marek Mošať are with the Institute of Electrical Engineering SAS, Slovak Academy of Sciences, 841 04 Bratislava, Slovakia.

Color versions of one or more figures in this article are available at https://doi.org/10.1109/TASC.2025.3546929.

Digital Object Identifier 10.1109/TASC.2025.3546929

I. Introduction

SUPERCONDUCTING cables represent a transformative advancement in power transmission technology, leveraging the unique properties of superconductors to facilitate the bulk and efficient transport of electricity over long distances with minimal energy loss [1], [2], [3]. This also has the potential to increase the reliability and capacity of electrical grids, addressing the growing demands for energy in the modern world. However, the successful implementation of these advanced materials in real-world applications hinges heavily on accurate circuit modelling, being it essential to predict the performance of superconducting cables under various operational conditions and to identify critical parameters such as temperature margins, magnetic field effects, and current-carrying capacity [3], [4], [5], [6], [7], [8]. Comprehensive models also play a vital role in optimizing designs, guiding maintenance strategies, and ensuring safety in power transmission systems.

The non-trivial structures of superconducting DC cables, the highly non-linear and multi-physics behaviour and the coexistence of different components with largely different aspect ratio and physical properties represent a challenge for modelling tools. This complexity, in fact, compromises the possibility of using complete analytical models but also leads to pitfalls for numerical approaches.

Finite element method (FEM) solvers allow very detailed analysis at the device level, but their complexity and computational burden makes it practically unfeasible for dealing with large systems involving many components.

Alternatively, the superconducting system can be investigated resorting to multi-physics circuit models, incorporating both thermal and electrical effects, in which the parts of the system of physical interest are described by lumped circuit elements [4], [9], [10], [11], [12], [13], [14]. They are characterised by simplicity and speed, require reduced computational resources and the offer the possibility to be used in power system simulators in combination with the detailed model of other system's components (converters, transformers, circuit breakers, surge arresters, etc.)

These models have been proved to be effective when the calculation of the circuit parameters is accurate.

These advantages make the circuit models of superconductor apparatuses particularly suitable for application to larger systems, whereby different components including power electronic converters and protection apparatus, driven by complex control

© 2025 The Authors. This work is licensed under a Creative Commons Attribution 4.0 License. For more information, see https://creativecommons.org/licenses/by/4.0/

strategy, must also be taken into account [15], [16], [17]. These circuit models integrate more easily with control system design methodologies, allowing leveraging existing tools and methods for control and protection strategy development [11], [12], [15], [16], [17].

Although circuit models of superconducting power cables are accurate and fast for reproducing the overall behaviour of the cable and its interaction with the hosting system, it is still essential to understand the detailed distribution of physical quantities within the cable, and in particular, the temperature [18]. This allows to precisely check the cable's design, evaluating any potential asymmetries and identifying regions that are more thermally stressed [19], [20]. Such insights are crucial for ensuring the reliability and longevity of the cable, as localized thermal stresses, especially during fault conditions or system transients, could affect performance [17]. By complementing circuit models with detailed FEM thermal analysis, a more comprehensive assessment of the cable's behaviour can be achieved, combining the speed and simplicity of circuit models with the detailed physics-based analysis of FEM, and still allowing the whole model to be included in large-scale system-level simulators.

Traditional combined Circuit-FEM methods solve the circuit and FEM simultaneously, ensuring real-time feedback between the two [21], [22], [23], [24]. This approach, however, still demands significant computational resources and is impractical for long-term or highly complex systems, such as large power infrastructures. Additionally, implementing the combined Circuit-FEM approach in popular power system simulators is non-trivial [21], [22], due to their limited flexibility, hence it mainly remains employed in FEM software packages [25], with limited possibility of implementing other crucial components (e.g., converters, control, protection, etc), or in home-made programming [24]. Finally, the coupled nature increases numerical complexity and the risk of instabilities, and validation becomes more challenging due to error propagation between subsystems.

In this paper a different approach to the combined Circuit-FEM modelling of a large power system involving a multi-layer superconducting power cable with high current capacity is used. The approach consists of cascading the circuit and FEM modelling, where the electrothermal circuit is solved first, and its results in terms of current profiles in the various cable's components, are used as input for the FEM. It is stressed that this circuit model is able to accurately account for the actual 3D layout of the cable, including twisting, that impacts both the inductances and the magnetic field acting on the tapes. This allows the reliable calculation of the currents of the layers which feed the 2D FEM model. These accurate current sharing could not be obtained with the 2D FEM modelling only.

The temperature calculation performed using the thermal circuit model is sufficient for determining the current distribution. However, the FEM analysis is required to refine the calculation and extract the temperature distribution to account for the geometric effects of individual conductors.

II. Combined Circuit-FEM Model of the Cable

The combined circuit model consists of two coupled dynamic nonlinear circuits, one electrical and one thermal, which

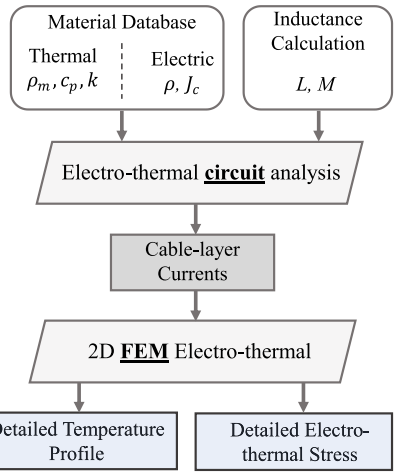

Fig. 1. Flow chart describing the adopted methodology.

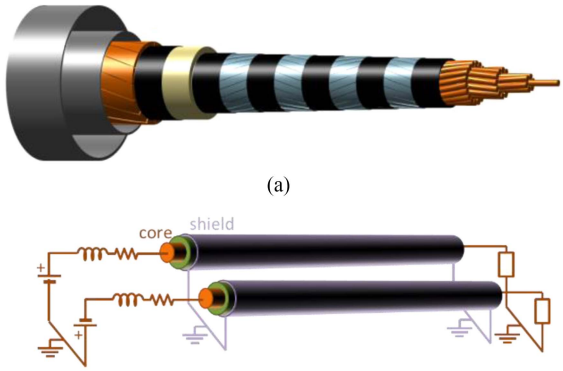

(a)

(b)

Fig. 2. Detailed HTS cable geometry (a) and schematic representation of the simulated HTS-HVDC bipolar transmission line (b).

consider temperature-dependent parameters and are capable of calculating the currents in the various cable elements (former, HTS layers, shield, pipes) [9], [10]. These calculated currents are used as input sources in the 2D electro-thermal FEM model to accurately assess the 2D distribution of the temperature. The combined Circuit-FEM modelling procedure is schematically depicted in Fig. 1 and is described in detail in the following.

HTS superconducting cables are composed of multiple layers of different materials, each made up of various wires or tapes. The typical structure of HTS cables consists of an inner copper core, known as the former, surrounded by multiple layers of HTS material. These HTS layers are separated by thin insulating layers, with an additional insulation surrounding the HTS stack. The assembly is further protected by a copper shield and embedded in cryogenic pipes to ensure the required cooling. The structure of the cable considered in this work is depicted in Fig. 2(a) and comprises a four-layer multi-filament copper former (inner, orange), four multi-tape HTS layers (light grey), the insulation (yellow), the shield (outer, orange) and the two pipes (dark grey). Specifically, the inner pipe contains the liquid nitrogen while the outer one serves as vacuum enclosure. The HTS layers and the shield are insulated from the adjacent layers

by carbon black sheets (depicted in black). The schematic of the combined circuit-FEM model is shown in Fig. 2(b).

A. Electro-Thermal Circuit Model

1) Electric Circuit: The parameters of the electrical circuit are calculated using analytical formulas, numerical techniques and databases, as shown in [9]. Each conducting element of the cable (former, HTS layers, shield, pipes) is modelled as an ohmic-inductive branch, which includes a nonlinear resistor in series with an inductor mutually coupled with all others. The inductance coefficients are calculated using the semi-analytical method described in [26], which is able to consider the precise geometric model of the individual helical conductors forming the layer. More in particular, the various layers are constituted by different conductors (tapes in case of the HTS layers and shield, wires in case of former) that after individual of resistance and inductance are merged into a unique homogenised layer, so that the electric equivalent circuit of Fig. 3(a) is obtained. In particular, for the generic ith and jth layer, the self and mutual inductance coefficients L_{ij} can be calculated as:

$$L_{ij} = \frac{1}{N_i N_j} \sum_{m}^{N_i} \sum_{n}^{N_j} L_{mn} \tag{1}$$

where L_{mn} is the inductance coefficient for the generic mth and nth tape or wire of layers m and n in the original cable geometry, and N_i and N_j the number of conductors of the ith and jth layers.

A detailed description of the model inductance behaviour is provided in [9]. It is stressed that since both the inductive and the ohmic parameters of the modelled cable layers are obtained from those individual conductors, modelled through their actual helical geometry, the effect of the twisting is taken into account in the circuit model.

For copper conductors, the resistivity is calculated as a function of temperature, while the resistivity of the SC HTS layers is obtained from the bounded power law, involving the parallel of a temperature-dependent "normal state" resistivity and the E-J power law SC resistivity, modelled using the well-known [27], [29], [30].

The resistances of the superconducting layer modelled as:

$$\rho_{HTS} = \frac{E_0}{J_c} \left(\frac{|\boldsymbol{J}|}{J_c} \right)^{n-1} \tag{2}$$

where E_0 is the critical electric field, n the exponential coefficient and J_c is the critical current density of the tape. This latter is expressed as a function of the temperature and the parallel $B_{\parallel}$ and perpendicular $B_{\perp}$ (to the tape) magnetic field components through a lookup table based on the typical experimental tests on a straight sample [27].

While the temperature of the tape is calculated through the thermal circuit, the magnetic field $\bar{B}$ at a certain time instant insisting on a HTS tape is obtained considering the overlap of magnetic fields generated by the currents in all layers, including non-superconductive ones. The contribution of the current from a generic jth layer to the ith layer is calculated at each time step by multiplying the jth current by means of numerically precomputed coefficients. These coefficients are obtained by first calculating the magnetic field in the reference frame fixed with the cable (with one axis aligned with it) and then projected in a cartesian reference frame fixed at any point with the tape for extracting $B_{\parallel}$ and $B_{\perp}$.

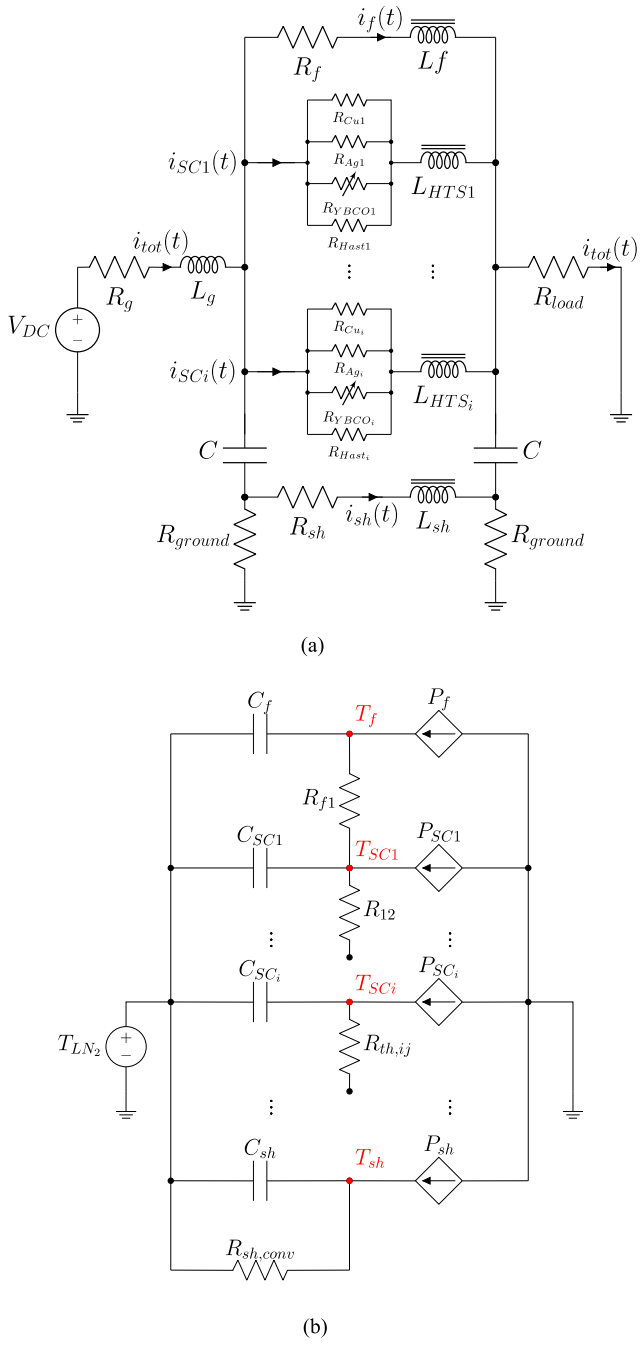

Fig. 3. (a) Electric and (b) thermal equivalent circuits of HTS power cables.

2) Thermal Circuit: To include the temperature effects and estimate the layer-temperature profiles during the transients the equivalent thermal circuit shown in Fig. 3(b) is coupled with the equivalent electric circuit. Each conducting layer is modelled through an equivalent thermal capacitance, estimated by merging the thermal capacity of all conductors of the layer into a unique as in [9]. In this work, the conductive heat transfer

among the layers and the convective heat transfer between the shield (external layer) and the cooling liquid are also considered. Specifically, thermal resistances are applied to the insulating and semiconducting layers between conductors, as these layers dominate heat transfer within the cable. By focusing on these layers, the model captures the key factors influencing temperature distribution. This simplifies the analysis while maintaining accuracy in representing the system's thermal behaviour. The thermal resistance $R_{th,\,ij}$ modelling the conductive heat transfer between the generic ith and jth cable layer is defined as:

$$R_{th,\,ij} = \frac{1}{2\pi k_{ij} l_{cable}} \ln\left(\frac{r_{int,j}}{r_{ext,i}}\right) \tag{3}$$

where k_{ij} is the thermal resistivity of the insulting material (electric insulation or carbon black) placed between the generic ith and jth cable layer, $r_{int,j}$and $r_{ext,i}$ are internal and external radiuses of the generic ith and jth cable layer, respectively, and l_{cable} the length of cable line.

Specific attention should be paid to the thermal resistance between the former and the innermost HTS layer. Indeed, the former of SC cables is composed of several filaments of round cross-section immersed in the cooling liquid, with can be considered stationary. In the manufacturing process the former's wires are compressed to ensure good adhesion of the carbon black to the layers and reduce the whole former diameter. This leads to a negligible heat transfer between the former and the coolant, hence this is not included in the thermal circuit of Fig. 3(b).

The heat transfer between the shield and the coolant id modelled through the convective thermal resistance $R_{conv,sh}$ defined as:

$$R_{conv,sh} = \frac{1}{2\pi r_{ext,cable} l_{cable} h_{conv}} \tag{4}$$

where h_{conv} is the convective heat transfer coefficient and $r_{ext,cable}$ the external radius of the shield in direct contact with the cooling fluid. As heat sources, the conducting-layer power losses are considered.

B. 2D Finite Element Model

The dynamic 2D FE model is designed to faithfully represent the geometric characteristics and components of the cable's cross-section which could not be considered through the thermal equivalent circuit. The model is fed with the current waveforms for each individual layer obtained by the equivalent circuit model, ensuring that the FEM analysis aligns closely with inductances dominated current distribution among cable elements. The time-dependent finite element electromagnetic model is implemented in COMSOL [33] and considers the cross-section of the cable as the 2D domain and solves the problem in the $\mathrm{A}-\varphi$ formulation:

$$E_z = -\frac{\partial A_z}{\partial t} - \frac{\partial \varphi}{\partial z} \tag{5}$$

where E_z, A_z are, respectively, the electric field and the magnetic vector potential along the axis of the cable, namely perpendicular to the 2D cable cross-section and $\varphi$is the electric scalar potential. Inherently to the 2D assumption, all sections along the cable length are the same, hence, the effect of the twisting, that impacts the distribution of current between the cables layer, is not directly taken into account in the FEM model alone. Nevertheless, this effect is considered in the combined circuit-FEM approach since all the layers of the cable included in the FEM model are fed with the proper layer current which is calculated through the circuit model that takes the twisting into account.

The assignment of the currents of each layer is achieved by imposing that

$$\int\int_{layer} J_z\left(\bar{B}, T, E_z\right) dxdy \; = i_{layer}^{circuit} \tag{6}$$

where $i_{layer}^{circuit}$ is the value of the layer current obtained with the circuit model and J_z the current density (in z-direction) depending on the local magnetic field $\bar{B}$, temperature T and electric field E_z.

In COMSOL (4) is implemented with the help of the electric potential φ. At each time instant, the value of φ in every current-transporting layer is based on a constraint, requiring that the total current through the 2D layer equals the current derived from the circuit model, namely enforcing (4).

In addition to the effect of the temperature on the HTS critical current, the model incorporates the influence of the magnetic field and its orientation with respect to the HTS tape. The implemented E-J characteristics is the power-law with the critical current depend on temperature and magnetic flux density according to (2).

The thermal problem is described by the 2D heat transfer equation:

$$\dot{\bar{q}} = \rho_m \, c_p \frac{\partial T}{\partial t} - k\Delta T \tag{7}$$

where $\dot{\bar{q}}$ is the heat-flow field, T the temperature and ρ_m, c_p, and k the mass density, specific heat and thermal conductivity of the medium, respectively. To model the cooling, the heat transfer through the outer boundary of the shield layer is considered, considering a constant heat transfer coefficient h.The detailed cable geometry used in the FEM model is shown in Fig. 4 (a), while Fig. 4(b) shows the whole FEM domain. A fictitious ideal and homogeneous conductor carrying the cable current is also included to model the interaction between the two monopoles of the considered power system (labelled as "return conductor" in Fig. 4(b)).

III. Case Study: The Scarlet Project

The SCARLET project is a Horizon Europe funded project with the key objective to prove the viability of using a medium voltage DC superconducting cable for transferring large amounts of offshore wind power to onshore locations, described in [1].

Various cable configurations utilizing HTS and MgB2 technologies were suggested, and in this study, the focus is on a two-monopole HTS system operating at +50 kV and −50 kV, with HTS cables designed to carry 10 kA. The power system architecture is shown in Fig. 5. This setup allows for

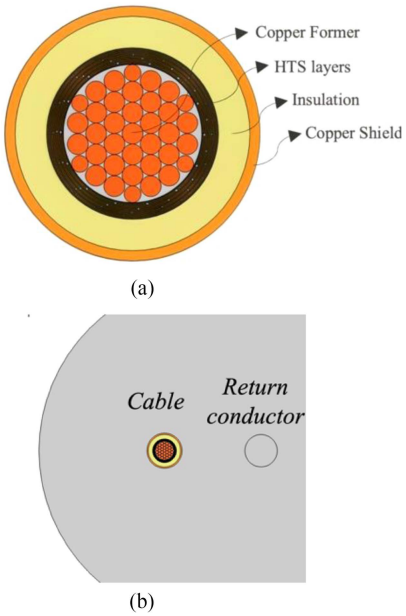

Fig. 4. 2D FEM model implemented in COMSOL Multiphysics of (a) the cable cross-section and (b) the whole domain with the cable cross-section and the fictitious return conductor.

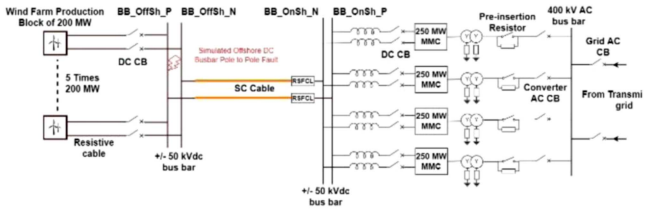

Fig. 5. Schematic of the considered microgrid, with specific indication of the pole-to-pole fault location.

the cryogenic fluid to be injected into one cable, with the return flow occurring in the other. Despite the compactness of the monopoles, the presence of strong electromagnetic fields around each pole will likely necessitate sufficient spacing between them for safe operation. Hence, a distance of one cable diameter is assumed between the two monopoles. The line parameters used in the circuit simulations are chosen to ensure the cable reaches the rated power in steady state operation. A solid bond scheme of the cable, assuming that the copper shield of both the monopoles is grounded at both the generator and load sides through the grounding resistances R_{groudn} (see Fig. 3(a)).

The HTS cable line is fed with two DC voltage sources of voltage V_{DC} with series resistance R_g and inductance L_g, emulating the Modular Multilevel Converter (MMC) converter used in the frame of SCARLET project [1] and, in general, in modern HVDC transmission systems [7], [31]. Attention should be paid to the MMC behaviour during the transients triggered by faults. Indeed, it in case of fault the converter switches are turned off, meaning that the switching units act as diodes. Thus, after the fault, the source can be modelled as a diode bridge in on state, i.e., MMC the flows through the diode resistances [32].

TABLE I
SIMULATION PARAMETERS

Parameter	Symbol	Value
Cable length	l_{cable}	100 km
Source voltage	V_g	50 kV
Source resistance	R_g	1 Ω
Source inductance	L_g	4.6 mH
Insulation capacitance	C	36.07μF
Load resistance	R_{load}	4 Ω
Grounding resistance	R_{ground}	1 Ω
Convection coefficient	h_{conv}	500 $\frac{\mathrm{W}}{\mathrm{m}^2 K}$
Fault time	t_{fault}	10 s
Fault resistance	R_{fault}	1 Ω

A. Transient Analysis and Results

As a case study, the energization transient and a pole-to-pole fault occurring when the line reached approximately steady-state conditions were analysed. This approach allows for the examination of the cable's behaviour under critical scenarios.

Specifically, the energization was simulated starting from an initial condition of zero current in the cable, and a fault transient was imposed after 10 seconds, a period considered sufficient for the cable currents (and overall system operation) to stabilize in steady-state conditions. After 60 ms the circuits breakers open the line suddenly making the current i_{tot}= 0 A while the other layer-currents are free to redistribute. The details of the simulation parameters are summarized in Table I.

The current distribution among the cable's layers calculated through the circuit model is plotted in Fig. 6(a) and clearly shows that by 10 seconds—the moment at which the pole-to-pole fault is triggered—the system has effectively reached a steady-state condition. Additionally, the figure reveals that during both the energization and fault events, the current distribution across the HTS superconducting layers is not uniform. This is due to the effect of self and mutual-inductance coefficients, which play a dominant role in shaping the transient electrical behaviour. This effect is particularly pronounced in superconductors where resistive contributions, which would impact the current distribution among layers, are negligible.

Moreover, Fig. 6 highlights that during the initial stages of both the energization and fault transients, the currents in some superconducting layers actually reverse direction.

To better visualise this peculiarity, a zoomed view of the cable currents is provided, specifically the energization transient in Fig. 7(a) and the fault transient in Fig. 7(b). Such behaviour is not only realistic but expected, given the cable's particular geometry, which leads to mutual inductance coefficients that are almost comparable to self-inductance coefficients, as previously discussed in [9].

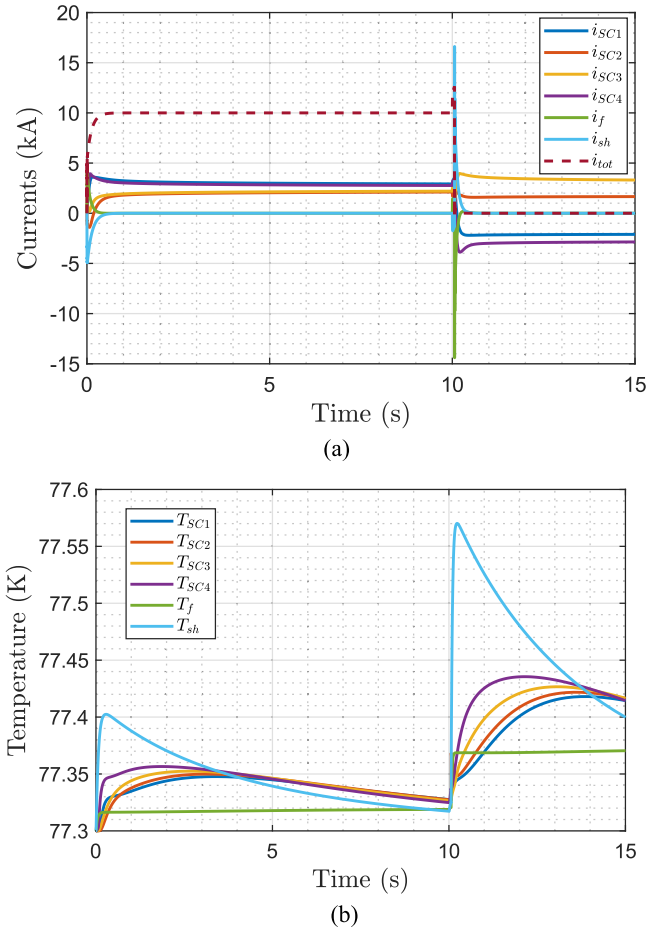

Fig. 6. (a) currents and (b) temperature profiles during the full transient (energisation and fault) obtained with the circuit simulations.

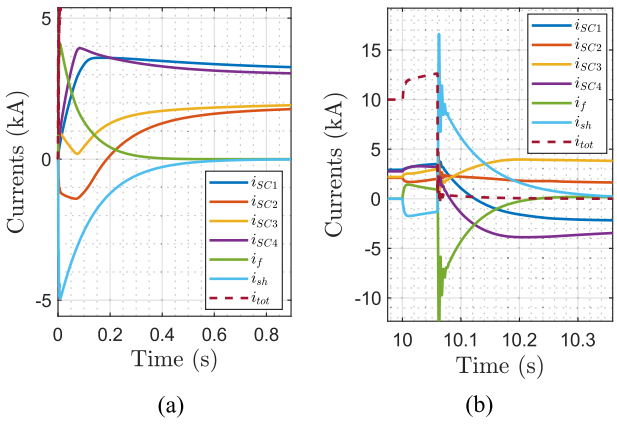

Fig. 7. Zoomed view of the cable currents during (a) the energization transient and (b) the fault transient.

The highest current experienced by the cable occurs during the fault transient. However, the individual HTS layers carry currents that exceed the nominal value of 2.5 kA by approximately 20% , assuming the total nominal cable current of 10 kA is evenly distributed among the four HTS layers. During the energization transient, the currents in the layers exceed the nominal value by up to 50% . This is particularly observed in the outermost layer (layer 4) and the innermost layer (layer 1). As expected,

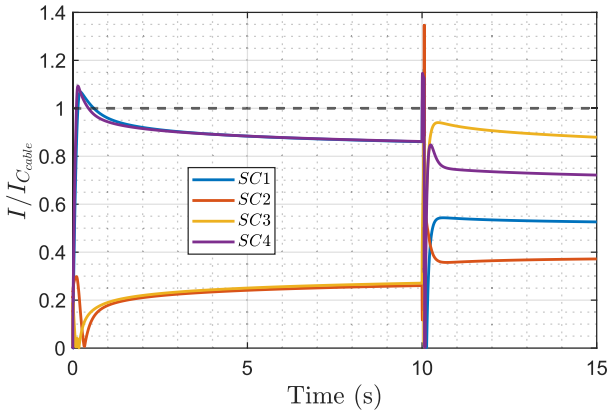

Fig. 8. Profiles of the ratio between the layer current and its critical value for the four HTS layers.

the currents in the former and the shield reach very high values (even exceeding the total cable current), effectively protecting the HTS layers. Under steady-state conditions (observable in the interval 2 s–10 s), the former and shield carry no current. It is also noteworthy that the former and the shield experience current peaks that are always opposite in sign. It should be noted that the grounding of the shield allows current circulation through it, which is closed through the grounding resistances R_{ground}, significantly influencing the current magnitude.

The value of R_{ground} has been selected based on the coordination requirements with the protections apparatuses of the power system and addressed at the system level [1], [9].

This behaviour is reflected in the temperature profiles shown in Fig. 6(b), particularly for the shield, which experiences the greatest temperature increase. The former, despite being subjected to significant currents, benefits from a larger overall cross-section immersed in the cooling liquid, which facilitates heat dissipation. The effects of energization and fault transients on the HTS layers can be effectively evaluated by observing the current they experience relative to their critical current. In Fig. 8, the behavior of I/I_c for the four HTS layers is plotted.

It can be observed that the current value (calculated considering the actual temperature of the layer at the corresponding instant) exceeds the critical current in both transients for layers 1 and 4, while for the other two HTS layers, it exceeds I_c only during the fault transient. However, I exceeds I_c for only very brief periods, insufficient to trigger cable quench, and the temperature remains within acceptable limits.

The overall temperature profiles of the layers obtained with the circuit model, as calculated in the FEM model fed with the current profile of Fig. 6(a), are shown in Fig. 6(b). At different time instants during the transient, it is observed that the temperature variation within the cable and the resulting overheating is minimal, with the maximum increase being approximately 0.15 K under the worst-case scenario. This moderate temperature rise is directly linked to the power losses. From the temperature profiles, it is evident that the outermost superconducting layer experiences greater dissipation, leading to a higher temperature increase compared to the other layers. In

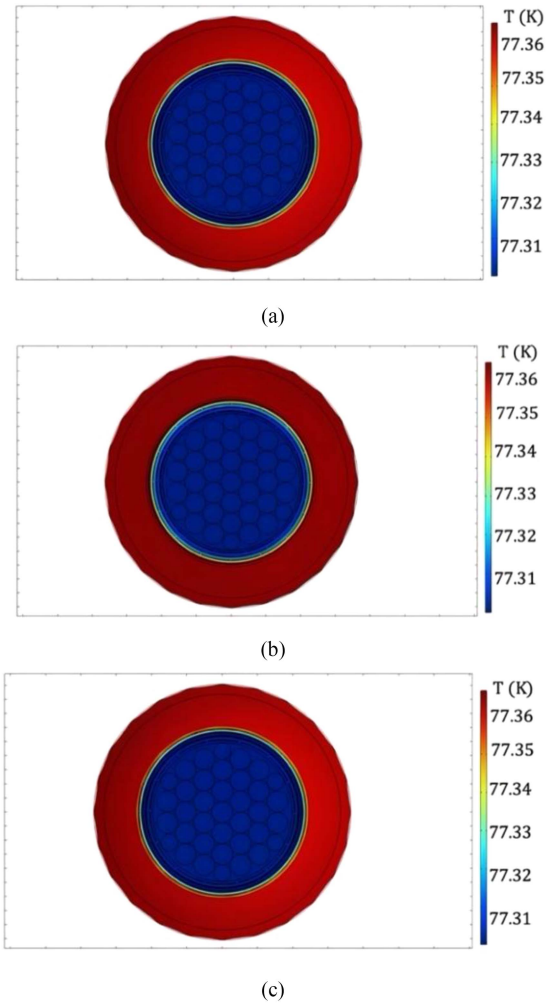

Fig. 9. Temperature-difference (with reference temperature $T_0 = 77.3$ K) in the cable cross-section during (a) the energisation transient (t = 0.6 s), (b) in steady-state (t = 9 s) and (c) during the fault transient (t = 10.6 s).

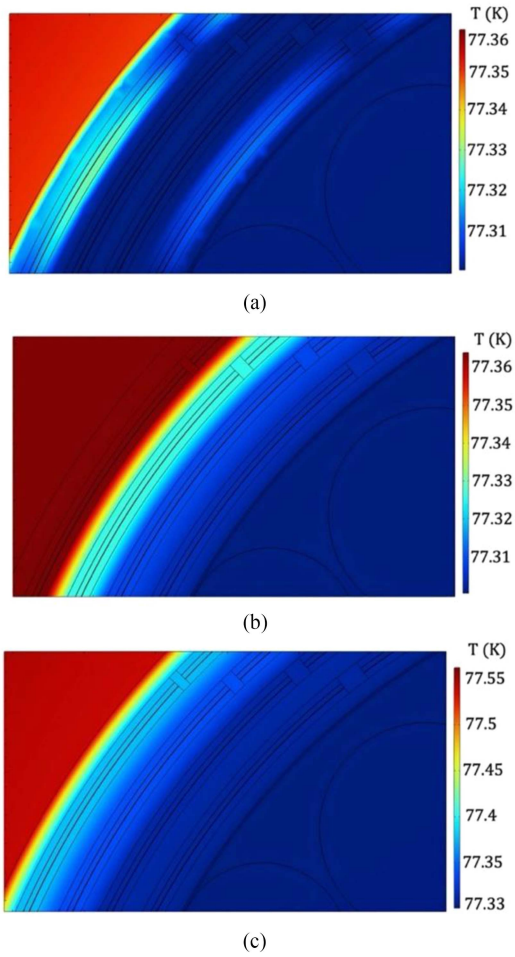

Fig. 10. Zoomed view of the temperature-difference (with reference temperature $T_0 = 77.3$ K) in the cable cross-section during (a) the energisation transient (t = 0.6 s), (b) in steady-state (t = 9 s) and (c) during the fault transient (t = 10.6 s).

contrast, the current in the copper former is significantly lower, resulting in minimal losses and a smaller temperature rise.

The thermal exchange between the layers, accounted for both in the circuit model and explicitly in the FEM model, remains contained and non-critical. Temperature maps across the cable cross-section are shown in Figs. 10 and 9 for key time points, including the initial energization transient (Figs. 10(a) and 9(a)), the steady-state period just before the fault (Figs. 10(b) and 9(b)), and the moments immediately following the fault (Figs. 10(c) and 9(c)). These temperature maps confirm the limited temperature increase experienced by the various layers of the cable, though they also highlight that this temperature variation is not completely uniform across the cross-section.

From the temperature distribution across the cable cross-section shown in Fig. 9, it is evident that during both the energization and fault transients—corresponding to Fig. 9(a) and (c), respectively—the temperature is not uniform across the section. This non-uniformity is attributed to the presence of the return conductor, as this is a bipolar line, which affects the current distribution and consequently the patterns of power losses and temperature rise. However, this variation remains minimal, with a maximum temperature differential of approximately 0.25 K under the worst-case scenario.

IV. Conclusion

A hybrid circuit-FEM simulation tool for the (time domain) transient analysis of HTS cables is presented and applied to the real case study defined in the European project SCARLET, which addresses the grid connection of 1GW power through a ±50 kV DC link. First, an electro-thermal circuit able to take into account the actual twisting of the conductors into the cable has been developed and proven to be effective and fast, thanks to the accuracy used for calculating the induction coefficients. A 2D dynamic FEM model of the cable-cross section has been then developed, able to calculate the detailed temperature distribution over the cable cross-section provided that the currents of each of the conducting element of the cable are assigned. The two models were combined by cascading them. More in particular, the circuit model was first run for calculating the current sharing between the layers and the FEM model, fed with the calculated currents, was the run for evaluating the detailed distribution of

the temperature within the 2D cross section of the cable. The results highlight that, despite the very moderate overall increase (max 0.25 K), a non unform distribution of temperature with the hottest point located on the shield at the outermost part of the cable. This confirmed the cable ability to resume operations even after a pole-to-pole fault, which represents one of the worst-case scenarios.

References

[1] N. Magnusson et al., "SCARLET – A European effort to develop HTS and MgB_2 based MVDC cables," *IEEE Trans. Appl. Supercond.*, vol. 34, no. 3, May 2024, Art. no. 5400205, doi: 10.1109/TASC.2023.3340646.

[2] G. Hajiri et al., "Design and modelling tools for DC HTS cables for the future railway network in France," *Supercond. Sci. Technol.*, vol. 35, Jan. 2022, Art. no. 024003,.

[3] L. Hu et al., "Insulation design of ±10 kV bipolar coaxial HTS DC cable," in *Proc. IOP Conf. Ser., Mater. Sci. Eng.*, vol. 768, 2020, Art. no. 062098.

[4] M. Yazdani-Asrami et al., "High temperature superconducting cables and their performance against short circuit faults: Current development, challenges, solutions, and future trends," *Supercond. Sci. Technol.*, vol. 35, no. 8, Jul. 2024, Art. no. 083002.

[5] J. H. Kim, M. Park, J. Cho, K. Sim, S. Kim, and I.-K. Yu, "Current distribution analysis of conducting and shield layers of HTS power cable under utility fault condition," *IEEE Trans. Appl. Supercond*, vol. 19, no. 3, pp. 1718–1721, Jun. 2009.

[6] A. Sadeghi, S. Seyyedbarzegar, and M. Yazdani-Asrami, "Investigation on the electrothermal performance of a high-temperature superconducting cable in an offshore wind farm integrated power system: Fault and islanding conditions," *IEEE Trans. Appl. Supercond.*, vol. 32, no. 8, Nov. 2022, Art. no. 5401011, doi: 10.1109/TASC.2022.3196770.

[7] W. Xiang et al., "DC fault study of a point-to-point HVDC system integrating offshore wind farm using high-temperature superconductor DC cables," *IEEE Trans. Energy Convers.*, vol. 37, no. 1, pp. 377–388, Mar. 2022, doi: 10.1109/TEC.2021.3094308.

[8] W. Xiang, W. Yuan, L. Xu, E. Hodge, J. Fitzgerald, and P. McKeever, "Fault transient study of a meshed DC grid with high-temperature superconducting DC cables," *IEEE Trans. Power Del.*, vol. 37, no. 6, pp. 5414–5424, Dec. 2022.

[9] C. Creusot et al., "Superconducting cable modelling into electro- magnetic transient simulation tool," *IEEE Trans. Appl. Supercond.*, vol. 34, no. 3, May 2024, Art. no. 5400606, doi: 10.1109/TASC.2024.3370118.

[10] W. T. B. de Sousa et al., "Thermal-electrical analogy for simulations of superconducting power cables," *Supercond. Sci. Technol.*, vol. 37, no. 9, Aug. 2024, Art. no. 095004.

[11] P. Chaganti, W. Yuan, M. Zhang, L. Xu, E. Hodge, and J. Fitzgerald, "Modelling of a high-temperature superconductor HVDC cable under transient conditions," *IEEE Trans. Appl. Supercond.*, vol. 33, no. 5, Aug. 2023, Art. no. 5400805, doi: 10.1109/TASC.2023.3251948.

[12] E. Tsotsopoulou et al., "Modelling and fault current characterization of superconducting cable with high temperature superconducting windings and copper stabilizer layer," *Energies*, vol. 13, 2020, Art. no. 6646, doi: 10.3390/en13246646.

[13] J. Zhu et al., "Mathematical modeling and current characteristics investigation of a 35 kV three-in-one high temperature superconducting (HTS) power cable," *IEEE Trans. Appl. Supercond.*, vol. 31, no. 5, Apr. 2021, Art. no. 5400704, doi: 10.1109/TASC.2021.3075271.

[14] T.-T. Nguyen et al., "A simplified model of coaxial, multilayer high-temperature superconducting power cables with Cu formers for transient studies," *Energies*, vol. 12, 2019, Art. no. 1514, doi: 10.3390/en12081514.

[15] X. Chen et al., "Simulation and analysis on the operational characteristics of the power transmission lines with a 110 kV/3 kA high temperature superconducting cable in a meshed grid," *Diangong Jishu Xuebao/Trans. China Electrotech. Soc.*, vol. 31, pp. 7–15, Aug. 2016.

[16] Y. Yokoo et al., "Temperature simulation of a 20 m HTS power model cable system in a fault current for 275 kV transmission lines," *IEEE Trans. Appl. Supercond.*, vol. 27, no. 4, Jun. 2017, Art. no. 5400906, doi: 10.1109/TASC.2017.2656621.

[17] P. Chaganti et al., "Transient analysis of HVDC HTS cable in power grid using discretized electrical-thermal model," *IEEE Trans. Appl. Supercond.*, vol. 34, no. 3, May 2024, Art. no. 4803806, doi: 10.1109/TASC.2024.3370896.

[18] W. T. B. de Sousa et al., *Supercond. Sci. Technol.*, vol. 34, 2021, Art. no. 015014, doi: 10.1088/1361-6668/abc2b0.

[19] X. Wu et al., "A simplified 2D modeling method for electromagnetic analysis of HTS power transmission cable spiraled with coated conductors," *IEEE Trans. Appl. Supercond.*, vol. 31, no. 5, Aug. 2021, Art. no. 4802106, doi: 10.1109/TASC.2021.3064791.

[20] J. He et al., "Thermal analysis of HTS power cable using 3-D FEM model," *IEEE Trans. Appl. Supercond.*, vol. 23, no. 3, Jun. 2013, Art. no. 5402404, doi: 10.1109/TASC.2013.2247651.

[21] W. Durante-Gómez et al., "FEM-circuit co-simulation of superconducting synchronous wind generators connected to a DC network using the homogenized J-A formulation of the Maxwell equations," *Supercond. Sci. Technol.*, vol. 37, no. 6, 2024, Art. no. 065021, doi: 10.1088/1361-6668/ad4a2f.

[22] W. Durante-Gómez et al., "Coupled FEM-circuit analysis of interconnected high temperature superconducting machines and components," in *Proc. 8th Int. Workshop Numer. Modelling High Temp. Supercond.*, Nancy, France, Jun. 2022.

[23] B. Zhang et al., "Field–Circuit cosimulation of 500-kV transformers in AC/DC hybrid power grid," *IEEE Trans. Appl. Supercond.*, vol. 26, no. 4, Jun. 2016, Art. no. 5500405, doi: 10.1109/TASC.2016.2529298.

[24] A. Pellecchia et al., "Development of a saturated core fault current limiter with open magnetic cores and magnesium diboride saturating coils," *IEEE Trans. Appl. Supercond.*, vol. 27, no. 4, Jun. 2017, Art. no. 5601007, doi: 10.1109/TASC.2016.2642147.

[25] G. dos Santos et al., *Supercond. Sci. Technol.*, vol. 34, 2021, Art. no. 045014, doi: 10.1088/1361-6668/abe600.

[26] F. W. Grover, *Inductance Calculations: Working Formulas and Tables*, Instrument Society of America, Reprinted by permission of Dover Publications, Inc., 1946 and 1973.

[27] WIMBUSH Database, Robinson Research Institute, Feb. 2019, [Online]. Available: https://htsdb.wimbush.eu

[28] J. Duron et al., "Modelling the E-J relation of high-Tc superconductors in an arbitrary current range," *Physica C*, vol. 401, no. 1-4, pp. 231–235, Jan. 2004.

[29] A. Morandi et al., "2D electromagnetic modelling of superconductors," *Supercond. Sci. Technol.*, vol. 25, no. 10, Sep. 2012, Art. no. 104003.

[30] A. Morandi et al., "Modeling of the resistive type superconducting fault current limiter for power system analysis and optimization," in *Proc. Presented at HTS Modelling Workgroup*, Bratislava, Slovakia, May 2014.

[31] H. Saad et al., "Dynamic averaged and simplified models for MMC-based HVDC transmission systems," *IEEE Trans. Power Del.*, vol. 28, no. 3, pp. 1723–1730, Jul. 2013.

[32] CIGRE, T. B. 604, *Guide for the development of models for HVDC converters in a HVDC grid* CIGRE WG B4-57, 2014.

[33] *AC/DC Module User's Guide*, COMSOL Multiphysics v. 6.2, COMSOL AB, Stockholm, Sweden, pp. 75–84.